
Investigations on the influence of antenna near-field effects and satellite obstruction on the uncertainty of GNSS-based distance measurements

F. Zimmermann, C. Eling, H. Kuhlmann
Institute of Geodesy and Geoinformation,
University of Bonn, Nussallee 17, Bonn, Germany
zimmermann@igg.uni-bonn.de

Abstract. Antenna near-field effects are one of the accuracy limiting factors on GNSS-based distance measurements. In order to analyse these influences, a measurement campaign at an EDM calibration baseline site with optimum GNSS conditions was performed. To vary the distance between the antenna mount and the absolutely calibrated antennas, spacers with different lengths were used. Due to the comparison of the resulting GNSS-based distance measurements to a reference solution, the influences of the antenna near-field could be analyzed.

The standard deviations of the differences to the reference solution, i.e., 0.31mm for the distance and 0.46mm for the height component, indicate that equal spacer and antenna combinations at both stations lead to a very high accuracy level. In contrast, different spacer and antenna combinations decrease the accuracy level. Thus, an identical set-up at both antenna stations and the usage of individually calibrated antennas minimize the near-field effects during the double-differencing process. Hence, these aspects can be identified as a prerequisite for highly accurate GNSS-measurements.

In addition to near-field effects, the influence of satellite obstructions is investigated. Four realistic shadowing scenarios are numerically simulated on the basis of the observations, which were collected in the optimum surrounding of the EDM calibration baseline site. The comparison to nominal values indicates that a shadowing leads only to a slight decreasing of the accuracy. Consequently, there is a strong suspicion that multipath effects and signal distortions seem to have a greater influence on the accuracy of GNSS-based distance measurements than the satellite constellation.

Keywords. GNSS, antenna near-field effects, satellite obstruction, EMRP JRP SIB60

1 Introduction

In Global Navigation Satellite System (GNSS) applications with high accuracy requirements at the millimeter level, like e.g., permanent reference station networks, the entirety of possible error sources has to be modelled, eliminated or prevented. Especially station dependent error sources, like e.g., multipath, antenna errors or satellite obstructions, are critical, since their effects depend on the antenna surrounding, the used antenna set-up and the antenna itself.

Theoretically, the estimated GNSS-positions refer to the antenna phase center, represented by one fixed point. In reality, the measurements depend on the direction of the incoming signal (azimuth α and elevation β). The deviations from the ideal mean phase center are described by the phase center variations (PCV) and the phase center offset (PCO). The latter one is the position of the mean phase center with respect to the antenna reference point (ARP) (Geiger 1988). To minimize the influences of unknown PCV and PCO parameters, GNSS antennas are commonly calibrated individually (Baire et al. 2014). In recent years, two procedures were proven to be the most effective approaches to calibrate GNSS antennas: the absolute robot calibration and a calibration in an anechoic chamber (Wübbena et al. 2000, Zeimetz and Kuhlmann 2008).

Other accuracy limiting factors are multipath effects, which can be separated into far-field and near-field effects. Far-field effects arise from reflecting surfaces in the environment of the antenna and lead to short-periodic errors. These short periodic errors can be averaged out by sufficiently long observation times (Seeber 2003). In contrast, antenna near-field effects result from the closest vicinity of the antenna, mostly described as the first 50cm around the antenna. On the one hand, near-



field effects can lead to a long-periodic error, which results in a non-zero mean distributed and unmodeled bias in the estimated parameters. On the other hand, the antenna near-field can change the overall electromagnetic properties of the antenna (Dilssner et al. 2008). Hence, individual antenna calibrations are actually only valid if the near-field situation has also been reproduced during the calibration procedure (Wübbena et al. 2006). This enables determining the influence of the antenna near-field on the phase center characteristics of the respective antenna. Furthermore, it leads to a more realistic site dependent calibration pattern (Dilssner et al. 2008, Wübbena et al. 2010). Nevertheless, size and weight limitations usually preclude a near-field calibration.

This paper answers the question, whether the influence of the near-field multipath can be minimized by increasing the distance between the top of the pillar and the antenna itself. Therefore, test measurements on an EDM calibration site were performed. Here, the distance between the antenna and the antenna mount was varied using different spacers.

Besides multipath and antenna effects, satellite obstructions are further site dependent error sources. Trees, buildings or other physical structures can lead to a shadowing of GNSS-signals and to a change of the satellite geometry at the respective station. In practice, usually the *Dilution of Precision (DOP)* values, which can be determined using the cofactor matrix of the position estimation, are a measure for the quality of the satellite-receiver geometry (Hofmann-Wellenhof et al. 2008).

In this study, satellite obstructions are numerically simulated by eliminating specific satellites of datasets measured at an optimum surrounding.

The remainder of the paper is structured as follows: Section 2 describes the field experiments and section 3 the results of the investigations on the near-field issue. In section 4, satellite obstruction scenarios are explained and the respective results are presented. Based on the results of sections 3 and 4, section 5 draws a conclusion and gives an outlook on further investigations.

2 Field experiments

In order to investigate the influence of antenna near-field effects and to prepare a basis for the simulation of satellite obstructions, a measurement campaign on the EDM calibration baseline site of the University of Armed Forces in Munich was performed. The calibration baseline site consists of eight pillars, placed on an earth-mound, with distances between 19 and 1100 metres (Heister 2012). The height differences between the pillars are less than 30mm and each of the pillars has a height of approximately 1.6m. Since there are no obstacles in the vicinity of the antenna, the GNSS-measurements can be performed under optimal GNSS measurement conditions. In particular, this includes a nearly multipath-free environment 3 to 4 metres above the surrounding surface level and a nearly free horizon.

During the measurement campaign, seven pillars were equipped with different antenna mounts. Spacer types with different lengths of 20, 40 and 60cm were used (cf. Fig.1) considering two aspects: (1) increasing the distance between the top of the pillars and the GNSS antenna and (2) reducing the influence of the antenna near-field.



Fig. 1 Set-ups for Leica AT504GG Choke Ring antenna.

Within the test measurements, three kinds of geodetic antennas were used (Trimble Zephyr Geodetic, Trimble Zephyr 2 and Leica AT504GG Choke Ring). All these antennas were individually calibrated for their PCOs and PCVs in the anechoic chamber of the University of Bonn (Zeimetz and Kuhlmann 2008).

In 8 observation sessions with durations of at least 4 hours, 162 baselines were observed with different antenna set ups. For the evaluation, the baselines were divided into two datasets. The dataset *equal*

(38 baselines) contains all baselines with equal spacer and antenna combinations, e.g., 20cm spacers and Trimble Zephyr Geodetic antennas, at both pillars. The dataset *mixed* (124 baselines) contains all mixed spacer and antenna combinations.

The most crucial point during the whole measurement process was the careful levelling and centering of the antenna spacer over the reference point of the pillar. Remaining uncertainties in this process can lead to a tilting of the antenna spacers causing deviations up to several millimeters in the estimated baseline length. Generally, the height component of the baseline is affected less by a tilting of the spacer. To avoid, or at least minimize these deviations, two rectangular arranged tachometers (Leica TS06) were used in a very time-consuming process to control the levelling and centering of the antenna spacers before and after every observation session.

3 Evaluation of the Antenna Near-Field

The GPS-baseline analysis was carried out using the standard post-processing software Leica Geo Office (LGO). Besides individual antenna calibrations, a standard ionosphere model and the Hopfield troposphere model were applied. To analyse the influence of near-field effects on the accuracy of GNSS-based distance measurements, the baselines, separated into distance and height component, are compared to known reference values. These reference values were determined with superior accuracy during an intercomparison programme in 2012 (Heunecke 2012).

Dataset equal In Figure 2, the mean differences in distance and height for dataset *equal* are displayed, sorted by the respective baseline lengths. For a better visualization, they are color coded. In addition, the antenna types used for each baseline are denoted (Z1: Trimble Zephyr Geodetic; Z2: Trimble Zephyr 2; L: Leica At504GG Choke Ring). Figure 2 shows that all differences to the reference solution are less than one millimetre in both components, except for the results of the baseline with the length of 18.7805mm and the spacer combination 60-60 (1.23mm). Furthermore, in relation to the spacer combinations 0-0, 20-20 and 40-40, the distance differences of baseline lengths

146.1469m and 177.9788m increased by about 0.65mm and 0.5mm when 60cm spacers were used.

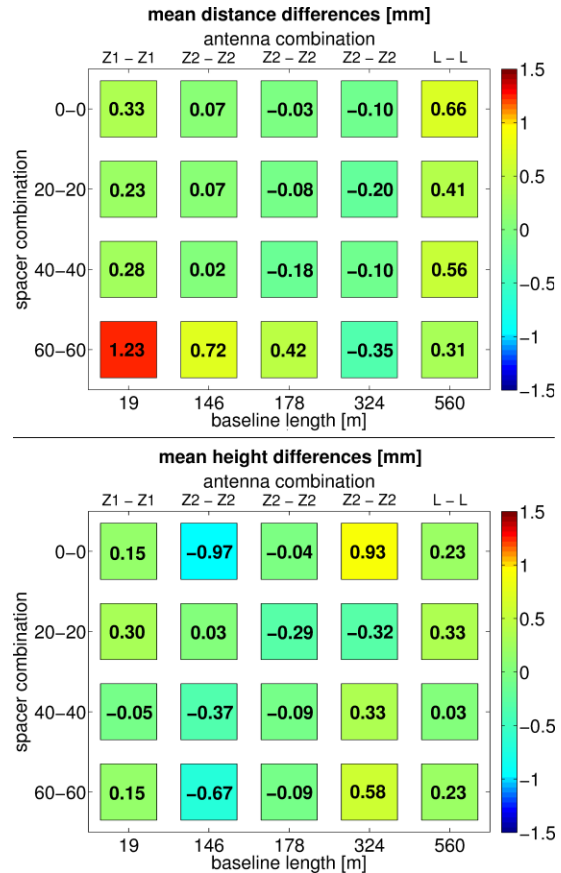


Fig. 2 Distance differences (top) and height differences (bottom) for dataset *equal*.

This indicates that despite the huge effort, the process of centering and levelling of the antenna spacers (cf. section 2) gets critical from a certain spacer height. Therefore, all baselines, where 60cm spacers were used, are not considered in the further analysis. For the remaining differences, no systematic effect is visible, neither related to the baseline length nor related to the different spacer lengths. Furthermore, no influence of the different antenna types used at the pillars can be detected.

Concluding, the length of the spacer does not affect the accuracy of the GNSS-based distance measurements at baselines with equal spacer and antenna combinations. Without differentiating between different spacer and baseline lengths, the mean value of the distance differences Δd , the mean value of the height differences Δh and the respective

standard deviations σ_d , σ_h are computed. This leads to $\Delta d=0.14\text{mm}$ and $\sigma_d=0.31\text{mm}$ for the distance component and to $\Delta h=0.02\text{mm}$ and $\sigma_h=0.46\text{mm}$ for the height component, respectively. The computed values emphasize the very high accuracy level reached with equal spacer and antenna combinations.

Dataset Mixed In Figure 3, the distance and height differences of the datasets *equal* and *mixed* are displayed. Additionally, Table 1 compares the respective mean values and standard deviations.

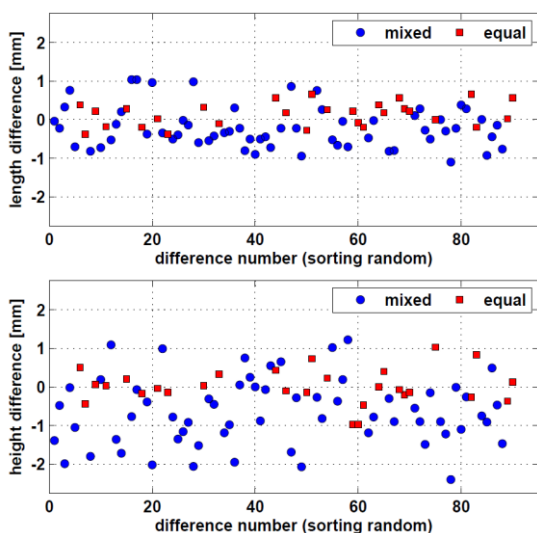


Fig. 3 Comparison of distance differences (top) and height differences (bottom) for datasets *equal* (red squares) and *mixed* (blue circles).

Table 1. Comparison of mean difference values and standard deviations for datasets *equal* and *mixed*

Distance component	mean [mm]	σ [mm]
<i>Equal</i>	0.14	0.31
<i>Mixed</i>	-0.21	0.53
Height component	mean [mm]	σ [mm]
<i>Equal</i>	0.02	0.46
<i>Mixed</i>	-0.65	0.87

Obviously, the values related to the distance component are less affected by different spacer and antenna combinations than the height component.

The distance differences of the dataset *mixed* vary between maximum values of 1.04mm and -1.10mm (cf. Figure 3). This leads to a mean value of $x=-0.21\text{mm}$ and a standard deviation of $\sigma_d=0.53\text{mm}$. For the height component, a mean value of $x=-0.65\text{mm}$ and a standard deviation of $\sigma_h=0.87\text{mm}$ are computed.

Comparison In comparison to the results of the dataset *equal*, the mean value of the distance differences of the dataset *mixed* is shifted by 0.35mm and the standard deviation is increased by a value of 0.22mm. The same trend applies for the height component of the baselines. Here, the mean value is shifted by 0.63mm and the standard deviation is increased by a factor of nearly 2.

The datasets *equal* and *mixed* only differ at their baseline lengths and their kind of spacer and antenna combinations. In dataset *equal*, the measurement set-up for the five observed baselines is completely identical in each case. The same spacer and antenna types were used at both pillars and the antenna cables were placed the same way. By comparison, in the dataset *mixed* different antenna types and spacer lengths were combined. Due to the short baseline lengths and the minimal height variation of the pillars, significant ionospheric or tropospheric effects can be excluded as a reason for the decreasing accuracy level. Otherwise they would become visible as a systematic length dependent effect (Spilker 1996). Hence, only the different spacer and antenna types at both stations can cause this deterioration, and thus, the increasing standard deviations and shifted mean values can be ascribed to the different near-field situations at both pillars. In conclusion, in the dataset *equal*, the influence of the antenna near-field is nearly similar at both pillars and can be minimized by the double-differencing process during the relative position estimation. Because of the different near-field situations in the dataset *mixed*, this is not possible.

4 Satellite obstruction

Obstacles in the signal path of GNSS-satellites lead to a shadowing of the signals and a deterioration of the satellite-receiver geometry. To analyze the influence of this deterioration on the accuracy of GPS-baselines, obstacles are numerically simulated in four obstruction scenarios.

4.1 Obstruction scenarios

Four real expectable shadowing scenarios are defined (*wall, tree, canyon and mining*). In these scenarios, the areas obstructing signals are bounded by certain values for azimuth and elevation. Since the data collected on the EDM calibration baseline site serves as a good basis for the simulation of satellite obstructions, the boundary values are related to the direction of the baseline site, east-north-east. To reach a preferably realistic simulation of the obstructions, their dimensions were determined using a tacheometer at comparable locations.

Scenario Wall In the scenario ‘wall’, both antennas are subject to satellite obstructions. They are induced by a long wall or dam in the same direction as the GNSS baseline, e.g., representing a noise barrier in areas of motor ways or railroad lines. These noise barriers can reach a height of about six metres. This leads to a shadowed area below 40 degrees elevation if the GNSS antennas are placed within a distance of seven to eight metres to the obstruction source. The azimuthal boundary is set to 75 and 255 degrees for each antenna, respectively.

Scenario Tree In the scenario ‘tree’, only one antenna is subject to satellite obstruction, induced by a big tree in the vicinity of this antenna. The height of the tree is assumed to be 13 to 14 metres. With a distance of about nine to ten metres between the GNSS antenna and the obstruction source, the shadowed area is below 55 degrees elevation. The azimuthal boundary depends on the tree width being set to ten metres in this case. This leads to an azimuthal boundary width of about 60 degrees.

Scenario Canyon In the scenario ‘canyon’, both antennas are subject to the satellite shadowing, induced by buildings forming an urban canyon. This represents one of the most popular shadowing scenarios in GNSS positioning (Groves 2011). For medium height buildings with three to four floors, the shadowed area reaches up to an elevation of 35 degrees. Assuming the direction of the urban canyon to be similar to the EDM calibration baseline direction, this leads to azimuthal boundary values of 80 to 240 degrees for the southern block

and 260 – 60 degrees for the northern block, respectively.

Scenario Mining In the scenario ‘mining’, both antennas are subject to satellite obstructions. In this case, the shadowing areas are different at each antenna. Possible examples of such a scenario are opencast coal mines or large construction sites. For antenna 1, the shadowing area reaches a maximum elevation of 40 degree in the western and a minimum of 12.5 degree in the eastern direction. For antenna 2, the elevation of the shadowing area is vice versa. Due to the circular characteristic of this scenario, there does not exist any azimuthal boundary value for both antennas.

In Figure 4, skyplots with the respective shadowing areas are depicted for each scenario.

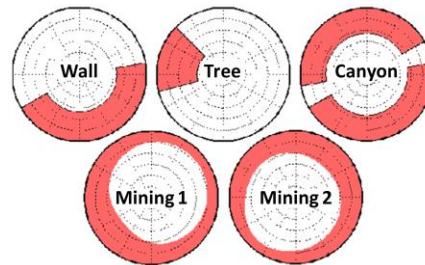


Fig. 4 Skyplots of obstruction scenarios with respective shadowing areas displayed in red.

4.2 Simulation procedure

For the simulation of the four obstruction scenarios, a simulation tool was implemented in Matlab[®]. Figure 5 depicts the simulation process schematically. In a first step, one has to choose one of the four predefined scenarios and the dataset, i.e., the respective RINEX-files, which shall be manipulated. In the next step, the RINEX-files are imported. Afterwards, an absolute single point position (SPP, Hofmann-Wellenhof et al. 2008) is computed to obtain the line-of-sight vectors of each satellite and, thereby, the azimuth and elevation of each satellite at every observation epoch. In the last step, the obstructed satellites are identified using the predefined shadowing boundaries of each scenario. Finally, the observations of the non obstructed satellites are used to rewrite the RINEX-files.

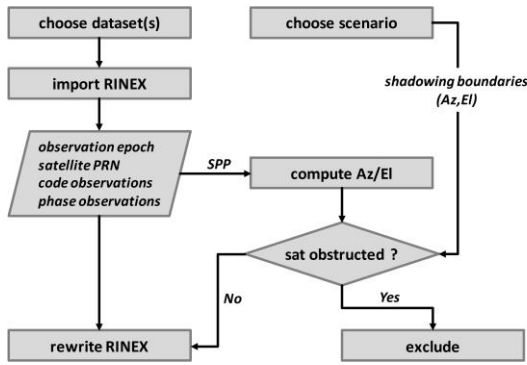


Fig. 5 Simulation process.

4.3 Evaluation

According to the result presented in section 3, only the baselines of the dataset *equal* are used for the simulation since these datasets represent observations with an optimum antenna set-up. All RINEX-files of the dataset are manipulated according to the process scheme depicted in Figure 5. Exemplarily, Figure 6 shows skyplots before and after the simulation of scenario *canyon* for one observation session at pillar 3.

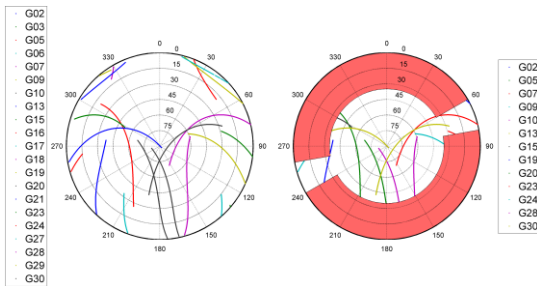


Fig. 6 Skyplots before (left) and after simulation (right) of scenario *canyon* for one observation session at pillar 3.

It can be seen that the total number of visible satellites is reduced from 21 to 13 in this case. To get an impression of the influence of the obstruction scenarios on the satellite configuration over time, the respective DOP values and numbers of visible satellites are presented in Figure 7. On top of this figure, the number of visible satellites (blue) and the DOP values (PDOP red, HDOP green, VDOP cyan) are shown for the observation session before the simulation.

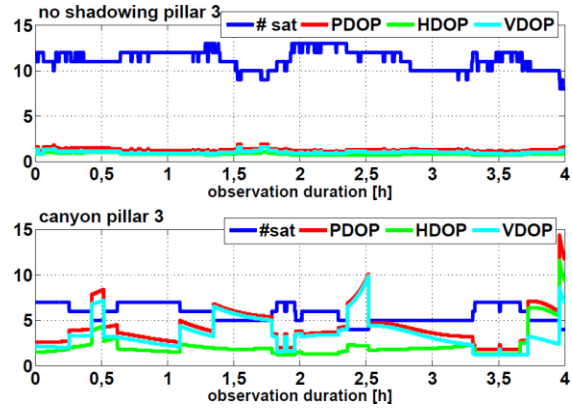


Fig. 7 Number of visible satellites (blue) and DOP values (PDOP red, HDOP green, VDOP cyan) for the non-shadowed case (top) and scenario *canyon* (bottom).

All DOP values are lower than 2. This emphasizes the excellent GNSS conditions at the EDM calibration baseline site.

In Figure 7 (bottom panel), the same values are shown for the scenario *canyon*. In this scenario, the number of visible satellites is nearly half of the number of visible satellites in the original dataset. Moreover, the PDOP and VDOP values increased to values above 5. Anticipating the results, it is noticeable that the HDOP value (green) is nearly unaffected by the satellite obstruction. The same applies for the scenario *mining* (not shown here). In the scenarios *wall* and *tree*, the number of visible satellites is reduced. However, this does not lead to a significant deterioration of the satellite geometry (not shown here). The majority of DOP values vary around 3, which still represents a good satellite constellation (Hofmann-Wellenhof et al. 2008).

After the simulation, the baselines were analyzed again with LGO using the same parameter settings as described in section 3. Afterwards, the results were compared to the nominal values for the distance and height components. In Table 2, the mean values \bar{x} and standard deviations σ of the differences are shown for all scenarios. The non-shadowed case (cf. section 3) is denoted as scenario *Ref*. Additionally, the respective mean DOP values are listed in columns 6 to 8.

Obviously, in comparison to the non-shadowed case, the accuracy of the distance component is unaffected by this obstruction scenarios. The same holds for the height component.

Table 2. Mean values x and standard deviations σ of height and distance differences and mean DOP values for obstruction scenarios.

Scenario	Distance component [mm]		Height component [mm]		Mean DOP values		
	x	σ	x	σ	P	H	V
Ref	0.14	0.31	0.02	0.46	1.3	0.8	1.0
Wall	0.23	0.41	0.09	0.46	2.1	1.4	1.6
Tree	0.07	0.38	0.07	0.46	1.5	1.0	1.1
Mining	0.15	0.38	0.32	0.87	3.4	1.6	3.0
Canyon	0.21	0.40	0.13	0.60	4.2	2.2	3.5

Only the precision after the simulation of the scenario *mining* decreased to a value of $\sigma=0.87\text{mm}$. Moreover, a relation to the corresponding DOP values can be identified. Despite the higher values at several timestamps (cf. Figure 7), the mean values of the DOPs, computed for the entire observation duration, are still low (cf. Table 2). Only for scenarios *canyon* and *mining*, there are changes visible leading to DOP values between 3 and 4.2.

Presumably, the observation duration of 4 hours compensates the deterioration of the satellite constellation in these cases. In order to analyze the impact of the observation duration, the duration has been reduced to 1 and 2 hours for all baselines. Afterwards, the whole simulation process and the baseline analysis has been repeated for the truncated datasets. The results are shown in table 3. The reduction of the observation duration does not affect the accuracy of the distance component in any of the four scenarios significantly. For the height component, there is a slight decrease visible. Nevertheless, the standard deviation of the differences and thus, the repeatability of the coordinate solution does still not exceed a value of one millimetre. In conclusion, despite of a deteriorated satellite constellation, an observation duration of 1 hour is sufficient to reach a high accuracy at the millimetre level in case of high quality GNSS signals.

The quality of the received GNSS signals is the crucial point here. During the simulation of the presented scenarios, the signals themselves have not been manipulated. This implies that they are

still originating from measurements in an optimum surrounding.

Table 3. Mean values x and standard deviations σ of height and distance differences for different observation durations.

Distance component [mm]	Duration 4h		Duration 2h		Duration 1h	
	x	σ	x	σ	x	σ
Scenario						
Ref	0.14	0.31	0.16	0.41	0.15	0.38
Wall	0.23	0.41	0.18	0.42	0.16	0.41
Tree	0.07	0.38	0.04	0.42	0.01	0.44
Mining	0.15	0.38	0.12	0.43	0.14	0.43
Canyon	0.21	0.40	0.14	0.43	0.09	0.41

Height component [mm]	Duration 4h		Duration 2h		Duration 1h	
	x	σ	x	σ	x	σ
Scenario						
Ref	0.02	0.46	0.16	0.65	0.22	0.74
Wall	0.09	0.46	0.17	0.62	0.08	0.74
Tree	0.07	0.46	0.15	0.62	0.26	0.74
Mining	0.32	0.87	0.37	0.88	0.37	0.67
Canyon	0.13	0.60	0.37	0.67	0.37	0.71

However, in reality scenarios, satellite obstructions are usually accompanied by multipath effects, e.g., in scenario *wall* and *canyon*, or a reduction of the signal quality, e.g., expectable in scenario *tree*. Therefore, in scenarios having a perfect surrounding apart from the shadowing, the influence of the mere deterioration of the satellite geometry can be denoted as being marginal in comparison to the uncertainty of the baseline determination. Nevertheless, it should be noted that the negative impact can be significantly greater due to concomitant effects, like e.g., far-field multipath.

5 Conclusion and Outlook

In this paper, investigations on the influence of antenna near-field effects and satellite obstructions on the uncertainty of GNSS-based distance measurements have been presented. The data of a measurement campaign with different antenna setups at an EDM calibration baseline site with optimum GNSS conditions served as a good basis for the analysis of these effects. On the one hand, the location enables a separation of different

uncertainty sources. On the other hand, nominal values for the distance and height component are available with a superior accuracy. The results of the investigations on the near-field issue revealed: the keys to highly accurate GNSS measurements are an identical antenna set-up and individually calibrated antennas of the same type at both antenna stations. With this kind of setup, similar near-field effects are minimized during the double-differencing process of the baseline analysis, leading to a repeatability of $\sigma_d=0.3\text{mm}$ for the distance component and $\sigma_h=0.5\text{mm}$ for the height component. Since the calibrated PCV values differ by several millimetres for the same antenna type, individual calibration patterns cannot be neglected. Moreover, it turned out that a similar antenna set-up is more important than using antenna spacers intended to minimize near-field effects. However, a distinct quantification of the near-field effect was not possible during the investigations presented here. Consulting the studies of Schmitz (2004) and Wübbena et al. (2006), a conceivable approach in further investigations would be trying to calibrate the GNSS antennas including a preferably realistic representation of the antenna mount and pillar surface in the anechoic chamber. Aside from mechanical issues due to weight and size limitations, this could be an option to quantify near-field effects in a continuative measurement campaign with different antenna calibration patterns for each antenna.

Furthermore, four realistic shadowing scenarios were presented and simulated to analyze the influence of satellite obstructions. The obstruction simulation led to a deterioration of the satellite configuration. Contrary to our expectations, the influence on the accuracy could be identified as being marginal since the very high signal quality still remains after the simulation procedure. Hence, we now hypothesize that far-field multipath effects and signal distortions are more critical than a poor satellite geometry. However, this has to be proven in further investigations, by analyzing the impact of a poor signal quality in comparable scenarios.

In this paper, only GPS signals were used for the baseline analysis. Due to the increasing total number of visible satellites from other GNSS, especially GLONASS and Beidou, these signals should be integrated to determine their impact on the accuracy of GNSS-based distance measurements.

Acknowledgement These investigations are performed within the joint research project SIB60 “Surveying” of the European Metrology Research Programme (EMRP). The EMRP is jointly funded by the EMRP participating countries within EURAMET and the European Union.

References

- Baire, Q., Bruyninx, C., LeGrand, J., Pottiaux, E., Aerts, W., Defraigne, P., Bergeot, N., Chevalier, J.M. (2014). Influence of different GPS receiver antenna calibration models on geodetic positioning. *GPS Solutions*, Vol. 18, No. 4, pp. 529-539
- Dilssner, F., Seeber, G., Wübbena, G., Schmitz, M. (2008). Impact of Near-Field Effects on the GNSS Position Solution. In: *Proceedings of the 21st International technical Meeting of the Satellite Division of The Institute of Navigation (ION GNSS 2008)*, Savannah, Georgia, September 16-19, pp. 612-624
- Geiger, A., (1988). Einfluss und Bestimmung der Variabilität des Phasenzentrums von GPS-Antennen. *Mitteilung des IGP der ETH Zürich*, No. 43, Zurich, Institut für Geodäsie und Photogrammetrie an der ETH-Zürich
- Groves, P. (2011). Shadow matching: A new GNSS positioning technique for urban canyons. *Journal of Navigation*, Vol. 64, Nr. 3, pp.417-430
- Heister H. (2012). Die neue Kalibrierbasis der UniBW München. *Allgemeine Vermessungsnachrichten (AVN)*, Vol. 10, pp. 336-343
- Heunecke, O. (2012). Auswertung des Ringversuchs auf der neuen Kalibrierbasis der UniBW München zur Bestimmung der Sollstrecken. *Allgemeine Vermessungsnachrichten (AVN)*, Vol. 11-12, pp. 380-385
- Hofmann-Wellenhof, B., Lichtenegger, H., Wasle, E. (2008). GNSS-Global Navigation Satellite Systems: GPS, GLONASS, Galileo & more. Springer, Wien
- Schmitz, M. (2004). Near-Field Effects of a Car Roof on TPSHIPER_PLUS Phase Variations. *GEO++ White Paper*, Garbsen, Germany
- Seeber, G. (2003). *Satellite Geodesy*, 2nd edn, Walter deGruyter, Berlin
- Spilker, J. (1996). *Global Positioning System: Theory and Applications*, Volume II, AIAA, Washington DC
- Wübbena, G., Schmitz, M., Menge, F., Böder, V., Seeber, G. (2000). Automated Absolute Field Calibration of GPS Antennas in Real-Time. In: *Proceedings of the 13th International Technical Meeting of the Satellite Division of The Institute of Navigation (ION GPS 2000)*, Salt Lake City, UT, September 19-22, pp. 2512-2522
- Wübbena, G., Schmitz, M., Boettcher, G. (2006). Near-Field Effects on GNSS Sites: Analysis using Absolute Robot Calibrations and Procedures to Determine Corrections. In: *Proceedings of the IGS Workshop 2006 Perspectives and Visions for 2010 and beyond*, Darmstadt, Germany, May 8-12
- Wübbena, G., Schmitz, M., Matzke, N. (2010). On GNSS In-Situ Calibration of Near-Field Multipath. In: *International*

Symposium on GNSS space-based and ground-based Augmentation Systems and Applications 2010, Brussels, Belgium

Zeimetz, P., Kuhlmann, H. (2008). On the Accuracy of Absolute GNSS Antenna Calibration and the Conception of a New Anechoic Chamber. In: *Proceedings of the FIG Working Week 2008*, Stockholm, Sweden, June, 14-19